Article ID: 1006-8775(2024)01-0076-13

Characteristics of Lightning Activity in Southeast China and its Relation to the Atmospheric Background

ZHI Shu-lin (支树林)[1], ZHU Jie (朱　杰)[2,3,4], LIU Yan (刘　岩)[5,6], MAO Meng-ni (毛梦妮)[7]

(1. Jiangxi Meteorological Observatory, Nanchang 330096 China; 2. Key Laboratory of Radiometric Calibration and Validation for Environmental Satellites, National Satellite Meteorological Center (National Center for Space Weather), China Meteorological Administration, Beijing 100081 China; 3. Shanghai Typhoon Institute, China Meteorological Administration, Shanghai 200030 China; 4. Innovation Center for FengYun Meteorological Satellite (FYSIC), Beijing 100081 China; 5. Key Laboratory of Transportation Meteorology of China Meteorological Administration, Nanjing Joint Institute for Atmospheric Sciences, Nanjing 210041 China; 6. Key Laboratory of Meteorological Disaster (KLME), Ministry of Education & Collaborative Innovation Center on Forecast and Evaluation of Meteorological Disasters (CIC-FEMD), Nanjing University of Information Science & Technology, Nanjing 210041 China; 7. Jiujiang Observatory, Jiujiang, Jiangxi 332000 China)

Abstract: Based on the lightning observation data from the Fengyun-4A (FY-4A) Lightning Mapping Imager (FY-4A/LMI) and the Lightning Imaging Sensor (LIS) on the International Space Station (ISS), we extract the "event" type data as the lightning detection results. These observations are then compared with the cloud-to-ground (CG) lightning observation data from the China Meteorological Administration. This study focuses on the characteristics of lightning activity in Southeast China, primarily in Jiangxi Province and its adjacent areas, from April to September, 2017–2022. In addition, with the fifth-generation European Centre for Medium-Range Weather Forecasts reanalysis data, we further delved into the potential factors influencing the distribution and variations in lightning activity and their primary related factors. Our findings indicate that the lightning frequency and density of the FY-4A/LMI, ISS-LIS and CG data are higher in southern and central Jiangxi, central Fujian Province, and western and central Guangdong Province, while they tend to be lower in eastern Hunan Province. In general, the high-value areas of lightning density for the FY-4A/LMI are located in inland mountainous areas. The lower the latitude is, the higher the CG lightning density is. High-value areas of the CG lightning density are more likely to be located in eastern Fujian and southeastern Zhejiang Province. However, the high-value areas of lightning density for the ISS-LIS are more dispersed, with a scattered distribution in inland mountainous areas and along the coast of eastern Fujian. Thus, the mountainous terrain is closely related to the high-value areas of the lightning density. The locations of the high-value areas of the lightning density for the FY-4A/LMI correspond well with those for the CG observations, and the seasonal variations are also consistent. In contrast, the distribution of the high-value areas of the lightning density for the ISS-LIS is more dispersed. The positions of the peak frequency of the FY-4A/LMI lightning and CG lightning contrast with local altitudes, primarily located at lower altitudes or near mountainsides. *K*-index and convective available potential energy (CAPE) can better reflect the local boundary layer conditions, where the lightning density is higher and lightning seasonal variations are apparent. There are strong correlations in the annual variations between the dew-point temperature (T_d) and CG lightning frequency, and the monthly variations of the dew-point temperature and CAPE are also strongly correlated with monthly variations of CG lightning, while they are weakly correlated with the lightning frequency for the FY-4A/LMI and ISS-LIS. This result reflects that the CAPE shows a remarkable effect on the CG lightning frequency during seasonal transitions.

Key words: lightning; satellite and ground detections; atmospheric background; Southeast China

CLC number: P427.3 **Document code:** A

Citation: ZHI Shu-lin, ZHU Jie, LIU Yan, et al. Characteristics of Lightning Activity in Southeast China and its Relation to the Atmospheric Background [J]. Journal of Tropical Meteorology, 2024, 30(1): 76-88, https://doi.org/10.3724/j.1006-8775.2024.008

Received 2023-07-11; **Revised** 2023-11-15; **Accepted** 2024-02-15

Funding: National Natural Science Foundation of China (42175014, 42205137); Open Research Fund of Institute of Meteorological Technology Innovation, Nanjing (BJG202202); Joint Research Project of Typhoon Research, Shanghai Typhoon Institute, China Meteorological Administration (TFJJ202209); Innovation Development Project of China Meteorological Administration (CXFZ2023P001); Open Project of KLME & CIC-FEMD (KLME202311); Jiangxi MDIA-ASI Fund

Biography: ZHI Shu-lin, M.S., primarily undertaking research on lightning.

Corresponding author: ZHU Jie, e-mail: juliet0411@126.com

1 INTRODUCTION

Certainly, the technologies for acquiring lightning observation data include electromagnetic radiation signal observation and positioning (ground-based observation), and optical detection (satellite observations). Historically, our understanding of regional lightning characteristics has been primarily based on ground-based observations. Among these, cloud-to-ground (CG) lightning data continues to be one of the mainstays in monitoring and forecasting thunderstorm activities. It relies on electromagnetic waves induced by lightning return strokes to detect lightning and obtain information such

as lightning spatial distribution and charge characteristics. Large-scale real-time lightning detection originated from Arizona University (Holle et al. [1]) in the mid-1970s, and the National Lightning Detection Network began to provide real-time lightning information in 1989 (Cummins et al. [2]). In the 1990s, China initiated the development of a multi-station lightning detection technology and established a relatively dense lightning observation network. Currently, the China Meteorological Administration has built a network consisting of over 400 stations, with baseline distances of 100–200 km (Zhang et al. [3]), which can accurately provide lightning location information in most parts of China, achieving a lightning detection efficiency of 94% and an arithmetic mean location error of 710 m (Chen et al. [4]). In recent years, all-flash detection systems based on extremely low-frequency or low-frequency signals have been reconstructed one after another (Liu et al. [5]). Since 2010, China has also constructed lightning positioning systems for scientific research, including the Low-Frequency Electric Field Detection Array, Beijing Lightning Network and all-flash integrated positioning network (the University of Science and Technology of China) (Lyu et al. [6]), which have provided the necessary infrastructure for understanding the spatial characteristics of lightning activity.

In recent decades, considerable advancements in satellite technology have greatly enhanced our understanding of lightning. Since the 1990s, spaceborne sensors have provided high-quality lightning observations that makes it possible to quantify and map global lightning distribution, even over the open sea. However, although these observations ceased after the Lightning Imaging Sensor (LIS) of the Tropical Rainfall Measurement Mission effectively monitored lightning for more than 17 years (1995–2014), this observational mission has since concluded. The LIS mission of the International Space Station (ISS) uses a low-rate telemetry channel to provide real-time lightning data. It extends its coverage farther north and south, reaching up to 55°N and 55°S, as opposed to the Tropical Rainfall Measurement Mission. The ISS-LIS offers a spatial resolution of 4 km and a maximum latitude coverage of approximately 54.33°N to 55°S, and its high-quality datasets can be shared freely from 1995 to the present. Following the LIS on board polar-orbiting satellites, a geostationary satellite carrying the Geostationary Lightning Mapper was launched in the United States in 2016. The Geostationary Lightning Mapper was introduced improved techniques for filtering, lightning data splitting and image reconstruction (Bruning et al. [7]). In April 2016, China launched a new generation of geostationary satellite, Fengyun-4A (FY-4A), featuring the independently developed Lightning Mapping Imager (LMI), which filled a crucial gap in domestic space-based lightning detection (Yang et al. [8]). The data from the Geostationary Lightning Mapper, LMI and ISS-LIS show that the ISS-LIS data magnitude is 11–12 times the FY-4A/LMI data magnitude (Cao et al. [9]). Moreover, the spatial distribution and daily or monthly variation characteristics of lightning recorded by these sensors exhibit a consistency (Hui et al. [10]), but the LMI lightning has a shorter mean radiation range, typically confined to the Tibetan Plateau. Further investigation revealed that the horizontal detection error of the LMI in the case of a isolated group of thunderstorms is about 15 km, and the detection efficiency in daytime is moderately low (Liu et al. [11]; Zhu [12]).

The availability of multi-source lightning data, which includes CG and satellite-based lightning detection, has made it possible to conduct comprehensive analyses of the meteorological characteristics of lightning on a global scale. Virts et al. [13] first proposed global lightning climatology based on the grided data from the World Wide Lightning Location Network. The research highlighted that during the summer, the proportion of lightning events is highest, but the lightning density and monthly variations exhibit notable regional distinctions. For example, Lightning activity over the provinces and territories is greatest in the summer, varying from 98% to 76.8% of the annual activity in Canada and Romania, respectively (Kochtubajda et al. [14]; Antonescu et al. [15]). In contrast, the lightning occurrences in October–April account for 90% in Australia (Kuleshov et al. [16]), and the summer lightning activity from satellite-based observations accounts for 68% in China (Yuan et al. [17]). Lightning density decreases with latitude, and its high-value areas are consistent with the deep convection areas, both of which have the same seasonal variation characteristics. Lightning density can reach 36 fl km^{-2} yr^{-1} (Houze et al. [18]; Bürgesser et al. [19]), and it is closely related to topography, being higher in mountainous areas than in plains (Orville et al. [20]; Liou et al. [21]). However, there are exceptions. As indicated by satellite-based lightning data from 2008 to 2014, the lightning density between altitudes of 300 m and 1000 m in Southwest China is lower than that below 300 m and above 1000 m (Hui et al. [22]).

Substantial spatio-temporal variations in lightning density are also evident within different regions of China. The areas with lightning density over 9 fl km^{-2} yr^{-1} are primarily located in the Sichuan Basin, the Yangtze River Delta and the southeastern coast, and the diurnal variation of lightning density is distinct in these areas. In Beijing, both mountainous areas and plains experience the most intensive lightning activity during the day and at night (Wang et al. [23]), but the lightning density peaks at night in Sichuan Basin and its adjacent mountainous areas, which is different from other areas(Xia et al. [24]; Wang et al. [25]). Due to the influence of land-sea breezes (Zheng et al. [26]), the activity degree of deep convection over land and coastal areas is different. Besides, there is also a certain correlation between lightning activity and precipitation patterns. The lightning probability in a convective precipitation zone is more than 20 times that in a

stratiform precipitation area (Feng et al. [27]). During convective precipitation in low-lying areas, the correlation coefficient between lightning frequency and the rainfall amount of extreme precipitation events can be as high as 0.75 in April–May and as low as 0.55 in June–August (Xu [28]). Convective available potential energy (CAPE) is a forcing factor of thunderstorm activity accompanied by lightning (Zheng et al. [29]), influenced by the maximum wet-bulb temperature. In tropical areas, an increase of 3–4 °C in wet-bulb temperature can lead to a twofold increase in lightning frequency (Kuleshov et al. [16]). In the vertical direction, the size of the radar echo volume with reflectivity of >30 dBz in the temperature range between −30 °C and 0 °C correlates remarkably with lightning frequency, and most of the lightning frequency peaks earlier than the occurrence time of 30 dBz radar echo volume maximum, with the longest leading time of 96 minutes (Yu et al. [30]). Sea surface temperature affects the lightning intensity in maritime areas, and the correlation coefficient between them is 0.797, but the significance of the correlation between them is not obvious (Wang et al. [31]). These findings collectively provide valuable insights into the climatic characteristics of lightning activity, though certain areas remain underexplored.

Lightning activity is frequent in Southeast China, with lightning strikes of varying intensities reported annually, including isolated instances of severe or even fatal lightning strikes. Therefore, it is essential to analyze the characteristics of lightning activities in this area based on long-term data series. The FY-4A/LMI, the sole geostationary satellite equipped with lightning imaging equipment in the Northwest Pacific, has been operational for more than five years. It has provided satellite-based detection data for studying convective weather characteristics. By comparing the spatial distribution and temporal differences of satellite-based lightning and CG lightning, this study tries to investigate the differences between lightning prone areas and other areas in Southeast China. Furthermore, we aim to identify commonalities and distinctions in the detection results derived from multi-source data in this area. These analyses are intended to offer valuable insights for the advancement of refined disaster prevention and mitigation.

The remainder of this paper is arranged as follows. Section 2 introduces the data and methods used in this research. Section 3 shows the findings of our study. Conclusions and discussion are presented in section 4.

2 DATA AND METHODS

One of the primary sources of satellite-based lightning data is the FY4A/LMI 2 product provided by the National Satellite Meteorological Center of the China Meteorological Administration, which also includes the ISS-LIS data after quality control from the Global Hydrology Resource Center of the United States. These datasets all contain the basic output units: “event”, “group” data and lightning signal (flash) data. Specifically, “events” denote instances where the lightning imaging unit can detect a single pixel exceeding the environmental background threshold, and “groups” represent two or more lightning “events” in the same time frame, which further categorize the “events” based on specific time and spatial size thresholds. The “group” data, obtained through a clustering algorithm, is widely utilized for analysis. The CG lightning data can be obtained from the Tianqing system of the China Meteorological Administration. According to Carey et al. [32], lightning discharges with an intensity below 10 kA are regarded as non-CG lightning and are excluded. The dataset spans from April to September in 2018–2022.

The large-value centers of the CG and FY-4A/LMI data are consistent. However, the former exhibits a more scattered distribution, while the latter is more densely distributed and concentrated (Xu et al. [33]). In North China, the CG and FY-4A/LMI data are also consistent in the regional distribution and the differences in the number and occurrence time of lightning, yet the number of satellite-based lightning events is several to ten times greater than the number of ground-based lightning observations (Ren et al. [34]). The overall trends of the daily or hourly cumulative probability of the data from the Advanced TOA (time of arrival) and Direction system (ADTD) and FY-4A/LMI are the same. An innovative moving amplification matching algorithm applied to lightning data in Southwest China in July 2018 indicates that the average daily matching rate of the FY-4A/LMI observations is 63.23%, and the average surface distance between matched data points is 35.49 km (Li et al. [35]). It underscores the strong consistency between the matching rates of lightning position and number. The above studies are all based on quality-controlled data. The FY-4A and ISS-LIS lightning data are labeled as “1” (non-quality-controlled) and “2” (quality-controlled). The downloaded ADTD data were also quality-controlled by the Meteorological Observation Center of the China Meteorological Administration. Thus, this study directly adopts this quality-controlled data.

The lightning data from various sources are uniformly gridded into lightning density (the number of lightning strikes per square kilometer per year). To investigate the potential factors influencing lightning distributions and variations, the wind field and CAPE data of the fifth-generation European Centre for Medium-Range Weather Forecasts reanalysis data are also selected for analysis, with spatio-temporal resolutions of 0.25°×0.25° and 1 hour.

3 RESULTS

3.1 *Spatial distributions and variations of lightning activities*

Figures 1a–1c illustrate the lightning density distributions of the three data types. Notably, the lightning-prone areas for the FY-4A/LMI are in central

and southern Jiangxi Province, central and southwestern Fujian Province, and central and western Guangdong Province. The peaks more than 10 times are few and scattered in Jiangxi and Fujian, but they appear successively in Guangdong, implying that lightning activity is noticeably more frequent in Guangdong. Lightning density in northern Jiangxi is higher than that in northern Hunan and Zhejiang but lower in Hubei and Anhui. Fig. 1b reveals that the high-incidence areas of CG lightning are in eastern and southern Jiangxi, southeastern Zhejiang, central and eastern Fujian, and northeastern and western Guangdong. Among them, the coast of eastern Fujian is a large-value area of CG lightning density, with density values near Fuzhou City exceeding tenfold. The Wuyi mountain area is the large-value center of lightning density in Jiangxi, and the lightning density is lower in southern Ganzhou City and western Jiujiang City. The high lightning density areas in Jiangxi Province has a similar distribution to that in southeastern Hubei and southern Anhui, but larger than in eastern Hunan. Fig. 1c demonstrates that the lightning density for the ISS-LIS is low, which may be since the period for the ISS to pass through this area is shorter than that for the FY-4A geostationary satellite. The ISS-LIS lightning density is generally less than 2 fl km^{-2} yr^{-1}, and high-density areas are widely dispersed, encompassing central and southern Jiangxi, southeastern Hubei, eastern Fujian, and central and western Guangdong.

The lightning density distribution characteristics of the three data kinds are comparable. Specifically, the lightning density is higher in central and southern Jiangxi, central Fujian, and central and western Guangdong, and it is mostly lower in eastern Hunan. However, some distinctions also exist. Broadly, the high-value area of the FY-4A/LMI lightning density (Fig. 1a) is in inland mountainous areas. The lower the latitude, the higher the lightning density, comparable to the air temperature distribution characteristics. The high-value areas of CG lightning density (Fig. 1b) are primarily located in eastern Fujian and the coastline of southeastern Zhejiang, and the high-value areas of the ISS-LIS lightning density (Fig. 1c) are dispersed in inland mountainous areas and the eastern coast of Fujian. Compared with the altitude (Fig. 1d), it can be found that the mountainous areas in the eastern, central, and southern parts of Jiangxi, southeastern Zhejiang, and central Fujian are all lightning-prone regions. Most of the northern Yangtze River is relatively flat, and the lightning density in this region is typically lower than that in the southern part. Therefore, the mountainous terrain is closely associated with lightning-prone areas.

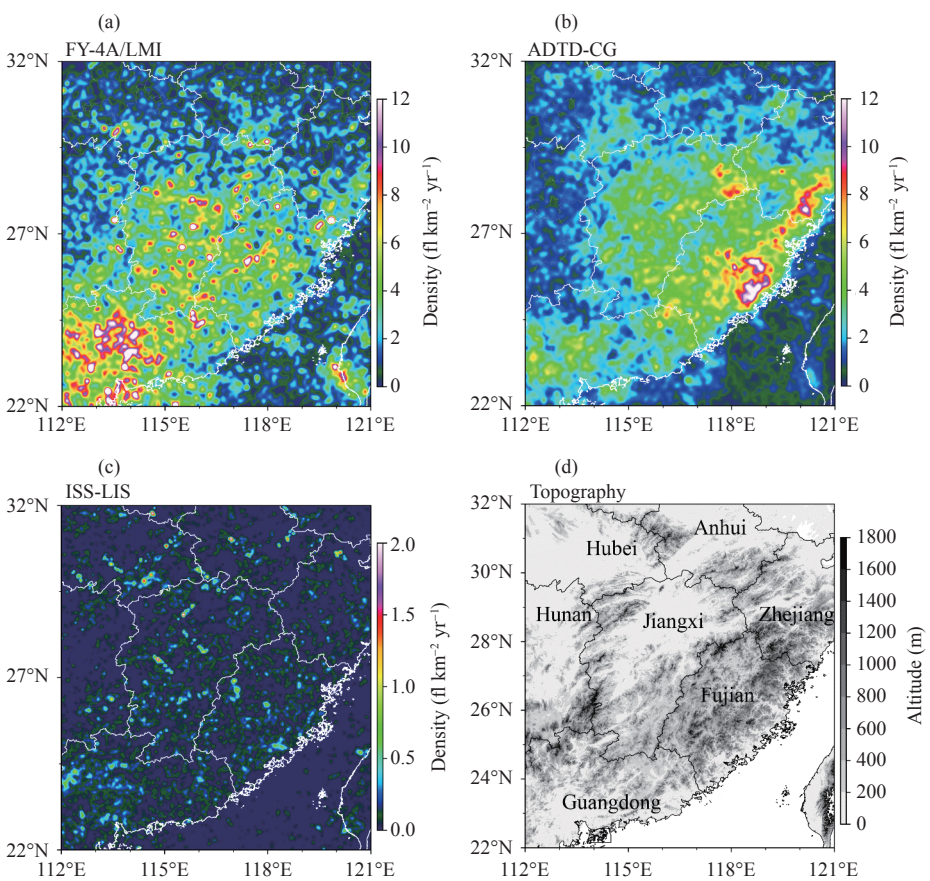

Figure 1. Lightning density (fl km^{-2} yr^{-1}) of the (a) Fengyun-4A/Lightning Mapping Imager (FY-4A/LMI), (b) Lightning Imaging Sensor on the International Space Station (ISS-LIS) and (c) Advanced TOA (time of arrival) and Direction system (ADTD) cloud-to-ground (CG) lightning data from 2018 to 2022, and (d) the latitude (m).

3.2 *Temporal variations*

3.2.1 MONTHLY VARIATION

The high-value lightning activity areas exhibit seasonal variations. Taking the FY-4A and CG lightning data as examples, Figs. 2a and 2b display the lightning density from April to September. The satellite-based lightning density in Jiangxi initiates an increase in April, and May–June are the most active months of lightning, especially in the central and southern parts of Jiangxi in May. The high-value areas of lightning density decrease in July, increases in August, and decreases rapidly after September. The distributions of lightning density in Guangdong and Fujian also demonstrate similar characteristics, i.e., the high-value areas of FY4A-LMI lightning density move northward in April–May, and the peaks appear in May and August.

The seasonal variation characteristics of the CG lightning density are more obvious (Fig. 2b). Compared with April, the CG lightning density in May–July increases obviously, and the high-value areas shift northward. August is still the high-incidence period of the CG lightning, but after September, the high-value areas of the CG lightning density rapidly move southward, and the lightning weakens. This variation is distinct from the findings of Zheng and Chen [26], who reported that the convective activities in South China in June are greater than that in July–August. This discrepancy is primarily associated with seasonal differences in the southern-central Jiangnan regions. From April to June, the heavy precipitation zones gradually shift northward, and in July, most of the southern Yangtze River and northern South China are controlled by the western Pacific subtropical high (WPSH), resulting in sunny and hot weather with no apparent regional convective activity. In August, due to the influence of the easterly system, lightning activities are often accompanied by heavy precipitation. After September, cold air activities from northern China gradually strengthen, and convective activities gradually weaken. In addition, lightning activity over the ocean is much less than that over land, reflecting the considerable influence of geomorphological characteristics.

There are similarities in the density patterns of the two lightning data types across seasons. Specifically, the locations of the high-density areas are predominantly overlapped, mostly in eastern and south-central Jiangxi, northern Guangdong, southern-central Fujian, and other places. The monthly variations are synchronous. May and September correspond to the northward movement and the southward movement of the high-density areas, respectively. However, there are also some differences. In July, the satellite-based lightning density is low, while the CG lightning density is high, notably in Fujian.

3.2.2 DIURNAL VARIATION

The hourly variation of the lightning frequency for FY-4A/LMI, ISS-LIS and CG lightning data are shown in Fig. 3. The results indicate that the CG lightning frequency is one order of magnitude higher than the FY-4A/LMI lightning frequency, and the latter is one order of magnitude higher than the ISS-LIS lightning frequency. This may be caused by the moderately low lightning detection efficiency of the FY-4A satellite in the daytime and the shorter efficient detection period of the ISS-LIS to Jiangxi and its surrounding areas (Liu [11]; Zhu [12]). The lightning frequency for the FY-4A/LMI has two peak periods: around 17:00–19:00 in the afternoon and around 04:00 in the morning. The lightning frequency for the ISS-LIS has roughly three peak periods: 15:00–16:00, around 20:00 and around 04:00 in the morning. In addition, the high satellite-based lightning frequency lasts for a long time, particularly for the FY-4A/LMI data which lasts until around 23:00. The CG lightning frequency decreases rapidly after 18:00. The satellite-based lightning observations include both local lightning and cloud lightning, and cloud lightning appears earlier and lasts longer. This phenomenon may be one of the reasons for the longer period of the high satellite-based lightning frequency. In the early morning, there is a slight jump in lightning frequency, necessitating further investigation.

Convective activities, as represented by lightning, have certain relationship with topography. Analyzing the sections of the FY-4A/LMI and CG lightning frequencies per hour along 116°E and 27°N, the results displayed in

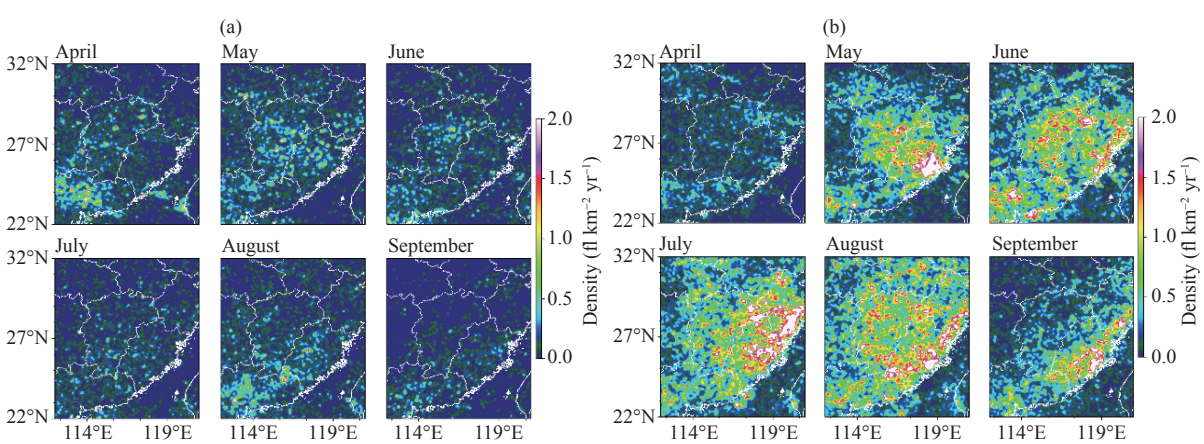

Figure 2. Monthly variation of the lightning density for (a) the FY-4A/LMI and (b) the CG.

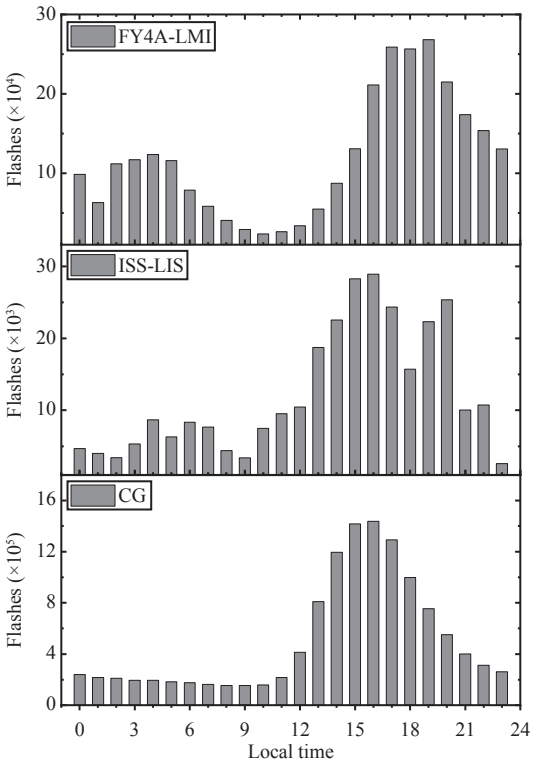

Figure 3. Hourly variation of the lightning frequency for the FY-4A/LMI, ISS-LIS and CG.

Figs. 4a–4b (FY-4A/LMI) and Figs. 4c–4d (CG) indicate that the lightning frequency of the two data types at the identical longitude and latitude appears mainly between 15:00 and 21:00. Comparing the locations of the frequency peaks of the two data types with the regional terrain latitude (dotted line in the figure), we find that these peaks are primarily located in low-lying areas or near hillsides, such as 24°N and 28°N in Fig. 4a, 115°E and 120°E in Fig. 4b, 25°N and 27°N in Fig. 4c, and 115°E in Fig. 4d. The potential reason for the higher lightning activity is that these areas have more convergence and ascending motion, which is easier to trigger orographic precipitation. Conversely, areas at the top of mountains do not exhibit such terrain features. This explains the moderately few topographic precipitation or convective activities in these areas.

3.2.3 ANNUAL VARIATION

In addition to the monthly and daily variations discussed above, convective activities indicated by lightning show evident quasi-climatic variations. Using the FY-4A/LMI and CG lightning data as examples, Fig. 5 presents the annual variation of lightning density. Fig. 5a reveals that, except for 2017, the areas where the lightning density of the FY-4A/LMI exceeds 2 fl km^{-2} yr^{-1} are mainly located in central and southern Jiangxi, western and southern Guangdong, and Fujian. However, the lightning density has gradually declined in recent years, particularly in 2022, primarily due to the sustained high temperature and less rainfall in the six provinces (or municipalities) of Anhui, Jiangxi, Hubei, Hunan, Chongqing, and Sichuan. In addition, the lightning detection performance of the FY-4A/LMI decreases year by year, which is another contributing factor to the decline in detection results. The annual variations of the CG lightning density (Fig. 5b) differ from that of the FY-4A/LMI results, i.e., the CG lightning density is higher in central and southern Jiangxi and Fujian in 2020, and

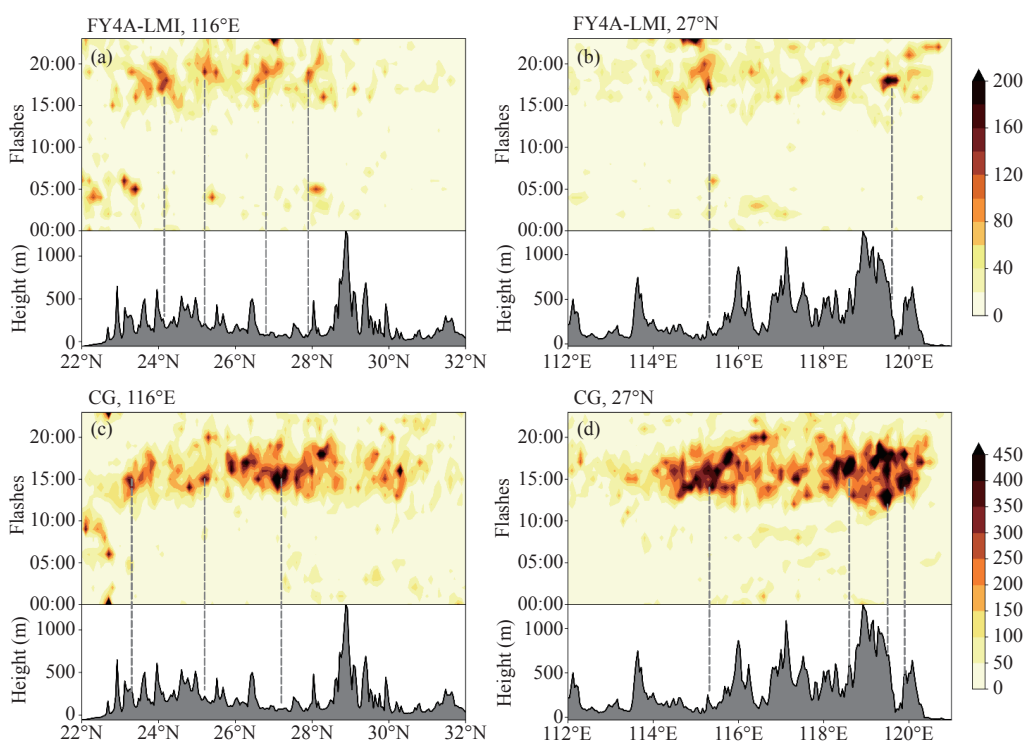

Figure 4. Daily variation of the hourly lightning frequency for the FY-4A/LMI and CG along 116°E and 27°N at different latitudes.

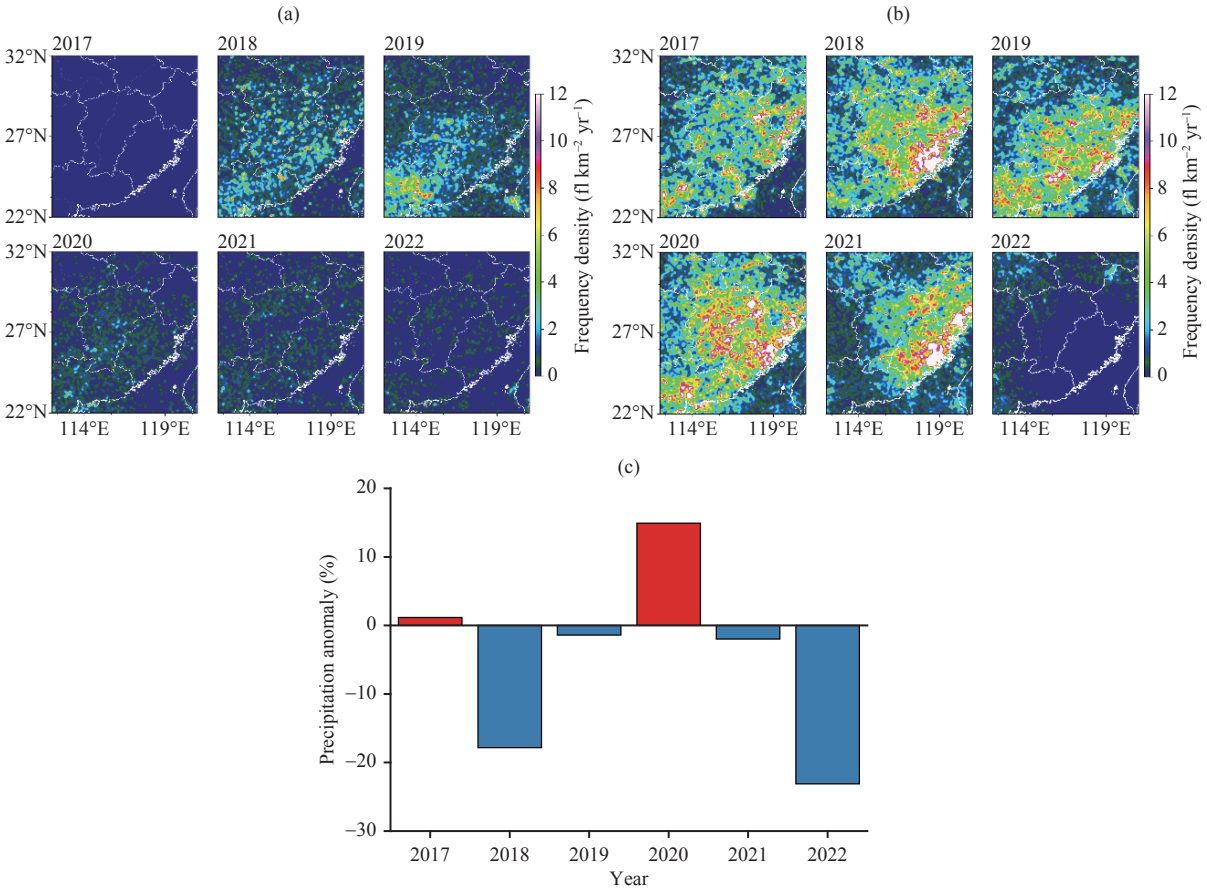

Figure 5. Annual variations of the lightning density of (a) FY-4A/LMI and (b) CG observations, and (c) the percentage of precipitation anomaly in Jiangxi.

additionally, it is higher in Fujian in other years of 2018, 2019 and 2021(the range of lightning density more than 5 fl km^{-2} yr^{-1}). In Jiangxi, the CG density commonly reveals annual variations, strengthening in 2018, weakening in 2019, strengthening again in 2020, and weakening again in 2021. Similar to the FY-4A/LMI results, the lightning density in Jiangxi, Fujian, Zhejiang and Guangdong in 2022 is exceptionally low, for the same reasons as mentioned earlier.

Figure 5c displays the variations in precipitation anomaly percentage in Jiangxi from April to September of 2017–2022. Apparently, negative precipitation anomalies appeared in 2018, 2019, 2021, and 2022, particularly in 2022, leading to a record drought event. The variation characteristics are consistent with the regional variations of areas with high lightning density in Fig. 5b. In other words, regions with more lightning activity in 2020 corresponded to increased precipitation.

3.3 *Relationship between lightning activity and atmospheric circulation background*

3.3.1 BACKGROUND CONDITIONS OF MONTHLY VARIATIONS OF LIGHTNING ACTIVITIES

Jiangxi and its surrounding areas are subject to monsoons, and the convective activities exhibit obvious seasonal variations. The monthly mean airflow field at 500 hPa and vertical velocity at 850 hPa from 2018 to 2022 (Fig. 6a) shows that the westerly wind prevails at 500 hPa in April, and areas with ascending motion of vertical velocity at 850 hPa are primarily situated in Guangdong and Fujian. After May, southern Jiangxi, Fujian, and Guangdong are controlled by southwesterly wind, and warm and humid airflow activities are accompanied by the strengthening and northward movement of the vertical velocity at 850 hPa. This circulation condition is favorable to the intensification of convective activities, which is also consistent with the increase of the FY-4A/LMI lightning density in southern Jiangnan and southern China (Fig. 2a). In June, the southerly component at 500 hPa increases. That is, the WPSH starts to uplift northward, and the lightning density decreases as the above areas are controlled by the WPSH. However, in central Jiangxi and other places, the ascending motion in lower layers is still maintained, and the lightning density in these areas is still moderately high. From July to August, the WPSH moves further northward, and the range of negative vertical velocity anomalies at 850 hPa gradually decreases. In July, since the WPSH controls most of eastern China, including Jiangxi, the convective activities are suppressed, and the lightning density further decreases. In August, the prevailing southwesterly wind shifts to the southeasterly wind in Jiangxi and its surrounding areas. Most of southern Jiangxi, Fujian and Guangdong are

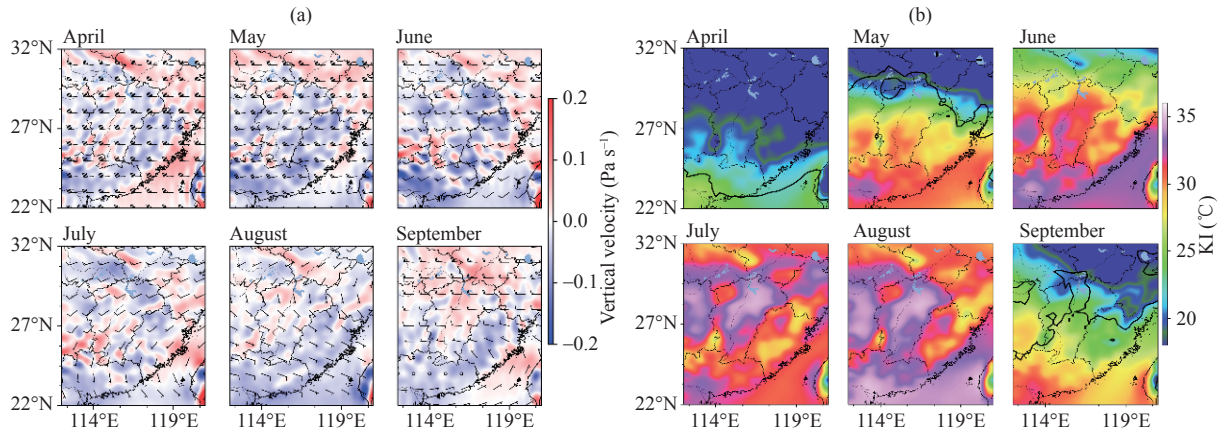

Figure 6. Comparison of the monthly (a) dynamic and (b) thermal conditions: (a) 500 hPa average wind field (bars) and vertical velocity (shaded areas), and (b) *K*-index (KI) (shaded areas) and the convective available potential energy (CAPE) of ⩾200 J kg^{-1} (isolines).

located on the southern border of the WPSH, and the lower level is dominated by negative vertical velocity anomalies, which is beneficial to convective activities. It is also consistent with the higher FY-4A/LMI lightning density in this area and lower density in others. After September, the WPSH moves southward, and the areas with high lightning density also shift to southern Jiangxi, Fujian, and Guangdong. The evolution of the median wind speed in the middle troposphere and the vertical velocity in the lower troposphere reflects the dynamic conditions of the seasonal variations of convective activities, which is consistent with the distribution of the FY-4A/LMI lightning density and its variations.

Thermal conditions represented by temperature and energetic conditions represented by the CAPE can also reflect seasonal variation characteristics and are closely related to the lightning density variation. Fig. 6b illustrates the variations in the *K*-index (KI) and CAPE. The areas with KI of ⩾25 °C in April are limited to southern Guangdong, and after May, they rapidly push northward to northern Jiangxi and Hunan and the intersection of Zhejiang and Fujian. From June to July, these areas continue to move northward until September, when the KI drops rapidly and the areas move to the vicinity of central Jiangxi and other places. This result reflects the fact that thermal conditions increase rapidly in May and then decrease after September. Similarly, the regions where the CAPE value exceeds 200 J kg^{-1} also show similar variation characteristics, and the isoline of 200 J kg^{-1} basically coincides with that of the 25 °C KI, implying that the variations in thermal and energy conditions are synchronous. Compared with the distribution and fluctuations of lightning density in the same period, it can be found that the areas where the lightning density for the FY-4A/LMI exceeds 0.25 fl km^{-2} yr^{-1} or the CG density exceeds 0.8 fl km^{-2} yr^{-1} basically coincide with the areas of the ⩾30 °C KI, suggesting that the variations of thermal or energy conditions have considerable influences on frequent lightning activities, especially during seasonal transitions. Besides, it is notable that there is no obvious correlation between areas with the high KI or CAPE and areas with the high lightning density from July to August. This is primarily since the thermal and water vapor conditions no longer play a critical role in determining the frequency of convective activities in the midsummer season when the WPSH is dominant.

Overall, the variations in the FY-4A/LMI lightning density are consistent with the northward strengthening and southward retreat of the WPSH, which is characterized by the prevailing wind in the middle layer. The specific values of the KI and CAPE can well reflect the boundary of regions with higher lightning density and its variations.

3.3.2 POTENTIAL CAUSES OF DIURNAL VARIATION DIFFERENCE IN LIGHTNING ACTIVITY

The data at 14:00, 17:00, 20:00 and 23:00 during 14:00–23:00 and that at 03:00, 04:00, 05:00 and 06:00 during 03:00–06:00 are taken for analyses. The CAPE distribution and the near-surface wind field at different times are shown in Fig. 7. The CAPE is the highest in the southeast coast and central Guangdong, followed by most of Jiangxi and northeastern Hunan in the afternoon, midnight, and early morning. The CAPE values in inland areas of Zhejiang and Fujian are lower. Additionally, the CAPE value is higher in inland areas of Jiangxi and near Dongting Lake in northern Hunan from afternoon to evening, and it is lower in the mountainous areas with high temperature around Jiangxi, most of Fujian and Zhejiang, and southern Hunan. After 20:00, the CAPE value increases in Poyang Lake, Dongting Lake and their surrounding areas, making these areas become isolated high-value centers in the early morning. The CAPE value decreases in other areas, which may be positively related to the surface air temperature. The air temperature gradually weakens after 05:00. The 850 hPa mean wind field shows convergence in central and southern Jiangxi from 14:00 to 20:00, and the convergence zone gradually shifts northward and then moves to Poyang Lake (116.3°E, 29.1°N) after 23:00. During 03:00–06:00, there is continuous wind convergence in Poyang Lake and its adjacent region, and the convergence area coincides with

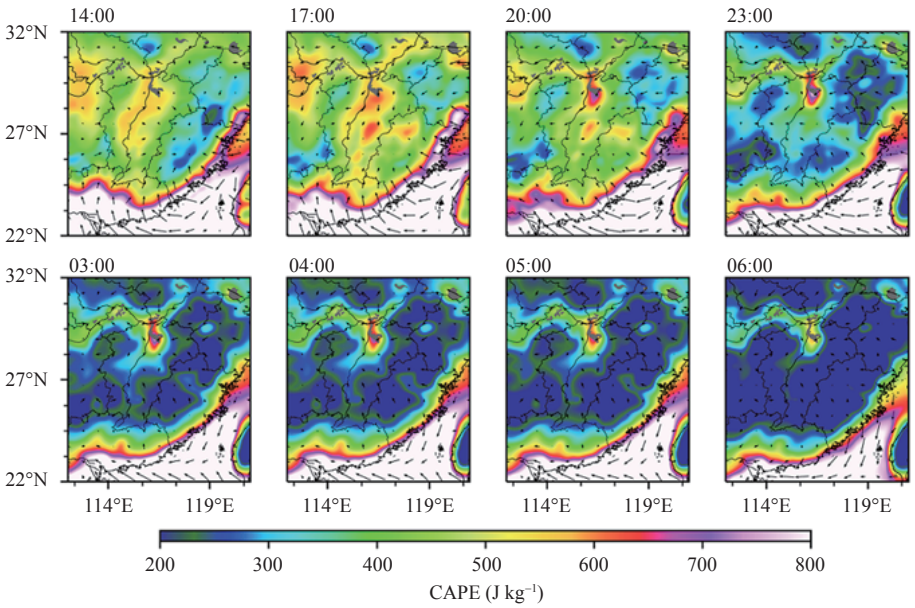

Figure 7. Hourly near-surface wind (bars) and the CAPE (shaded areas) at different times.

the area where the mean CAPE value exceeds 500 J kg^{-1}. This result reflects that the dynamic and thermal conditions near the lake area are better than those in other areas, conducive to convective activities in this area at night, which may be one of the reasons for the sudden increase in satellite-based lightning frequency in the early morning (Fig. 3). The lightning density distributions of FY-4A/LMI and CG observations at the same time (figure omitted) show that the lightning density in central and southern Jiangxi is higher during the afternoon and the first half of the night, which is roughly consistent with the CAPE high-value areas. In the early morning, the lightning density is higher in northern Jiangxi, particularly around Poyang Lake and its adjacent areas. The high-value areas of the lightning density coincide with the local CAPE high-value areas and the wind field convergence areas, indicating that the high CAPE and the wind field convergence have a good spatio-temporal consistency with the daily variation of lightning activity.

3.3.3 ASSOCIATED FACTORS INFLUENCING ANNUAL LIGHTNING ACTIVITY VARIATION

The annual lightning frequency of the three data types (Fig. 8a) indicates that the FY-4A/LMI lightning frequency peaks in 2017 and 2018, and then it decreases year by year. The variation of the ISS-LIS lightning is consistent with that of the CG lightning, i.e., the lightning frequency increases year by year from 2016 to 2018, decreases in 2019, increases again in 2020, and then decreases. The lightning frequency fluctuates considerably, which aligns with the spatial distribution characteristics of the lightning density presented in Fig. 5.

It is generally accepted that the variations of lightning frequency are induced by the variations of CAPE (Williams [36]). The relationship between lightning frequency and CAPE variation is virtually linear, as is the relationship with wet-bulb temperature (Rutledge et al. [37]; Williams et al. [38]). Fig. 8b displays the average air temperature (T), dew-point temperature (T_d) and the CAPE at the same time. It can be seen that the T_d annual variations are consistent with the ISS-LIS and CG lightning frequency variations, except for 2021, but they are different from the FY-4A/LMI lightning frequency variation. The Pearson correlation coefficients of the T_d with the FY-4A/LMI, ISS-LIS and CG lightning frequencies are 0.1, 0.5 and 0.63, with the significance test results of 0.8, 0.3 and 0.6, respectively. Thus, to a greater extent, the T_d is correlated with the CG lightning frequency. In terms of the annual mean value of the T, the surface temperature in the selected area fluctuated considerably in the last five years, and its variation does not agree well with the lightning frequency variation, with calculated correlation coefficients of 0.006, 0.04 and 0.38, respectively, with the FY-4A/LMI, ISS-LIS and CG lightning frequencies. This result suggests that there is no substantial correlation between the annual air temperature variation and lightning frequency, although the situation varies slightly in different years. For example, in 2018, the Pearson correlation coefficients of the air temperature and the lightning frequency of the above three data types are 0.14, 0.12, and 0.3, implying that air temperature has little influence on lightning frequency (especially for CG lightning).

The CAPE only increases in 2021, and it decreases in the other years. Its correlation coefficients with the FY-4A/LMI, ISS-LIS, and CG lightning frequencies are 0.02, 0.17, and 0.39, respectively, indicating a stronger correlation with CG lightning. However, the overall correlations are weak, and this relationship varies across different years. For example, in 2018, the correlation coefficients between the average CAPE and the above lightning frequencies of three data types are 0.38, 0.21 and 0.64, respectively, in the selected area, considerably higher

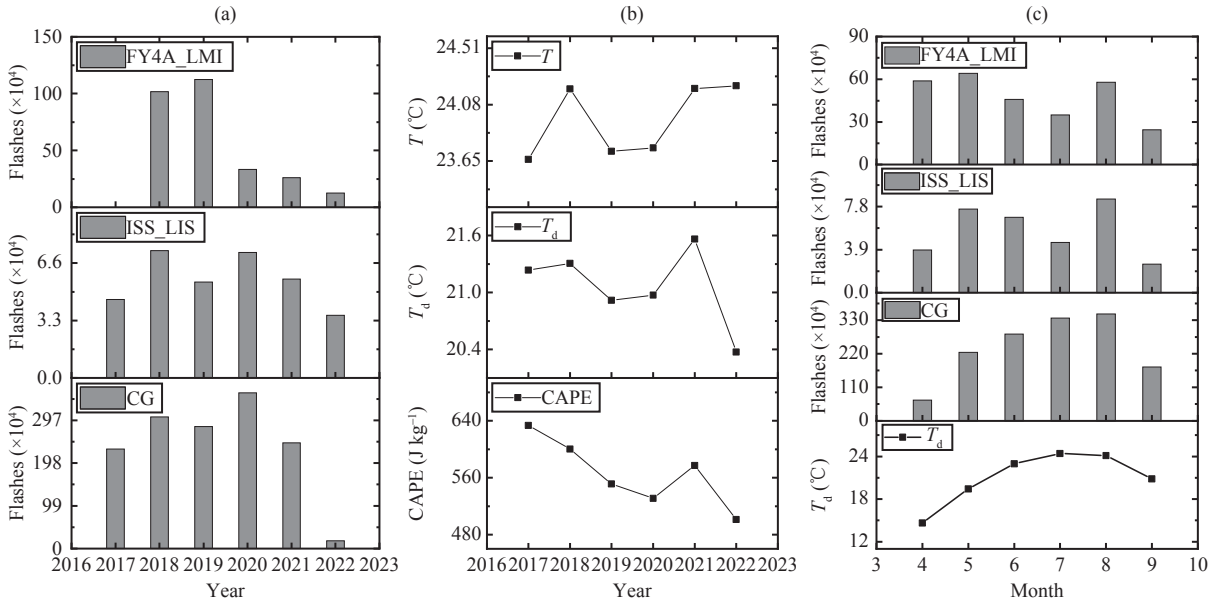

Figure 8. Annual variations of the (a) lightning frequency and (b) air temperature (T), dew-point temperature (T_d) and CAPE, and (c) their monthly variations.

than the five-year average. This underscores that the CAPE has a notable correlation with lightning frequency and exerts a more meaningful effect on lightning frequency than air temperature.

In order to gain deeper insights into the relationship between atmospheric environmental factors such as T_d and lightning frequency, we analyze the monthly mean T_d. As illustrated in Fig. 8c, the seasonal variation of T_d is fully consistent in that of the FY-4A/LMI and ISS-LIS lightning frequencies, i.e., increase in April, May and August, and decrease in June, July and September. However, the CG lightning frequency continues to increase before August and decrease after September. The correlation coefficients between T_d and the FY-4A/LMI, ISS-LIS and CG lightning frequencies are 0.38, 0.38, and 0.96, respectively. The correlation coefficients between the CAPE and the lightning frequencies are −0.29, 0.32, and 0.93. Thus, the correlations of T_d and CAPE with the CG lightning frequency are much higher than those with the FY-4A/LMI and ISS-LIS lightning frequencies. These findings are in line with similar research conducted in Australia (Kuleshow [16]).

In summary, the annual variations of the T_d and the monthly variations of T_d and CAPE are strongly correlated with the CG lightning frequency variation, but the correlations with the FY-4A/LMI and ISS-LIS lightning frequencies are weak, reflecting that the CAPE has a considerable influence on lightning frequency during seasonal transitions.

To delve further into the role of factors such as the CAPE in influencing lightning activity, the areas with CAPE values greater than 200 J kg^{-1} or KI greater than 32 °C are examined monthly and compared with the FY-4A-LMI and CG lightning frequencies. The results (Fig. 9) reveal distinct monthly variations in the FY-4A-LMI

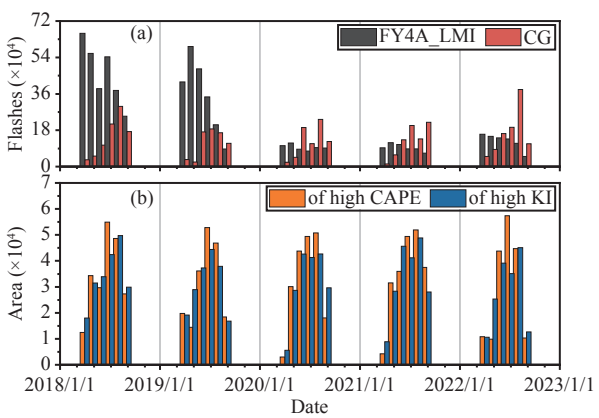

Figure 9. (a) FY-4A/LMI and CG lightning frequencies. (b) Areas of CAPE above 200 J kg^{-1} and KI over 32 °C.

lightning frequency, characterized by a gradual decrease. However, the CG lightning frequency increases first and decreases only in September, fluctuating between April and August. Contrastingly, the high-value areas of both the CAPE and KI areas demonstrate a pattern of increasing and then decreasing, but these variations are mostly earlier than those of CG lightning frequency, and the trend rate of the former exceeds that of the latter. For example, the high-value area of the CAPE decreases from 5×10^4 km^2 to 4.5×10^4 km^2 in July and August, 2022, but the CG lightning frequency increases from 1.9×10^5 to 3.8×10^5 in the same months in 2018. However, exceptions are noted, such as the synchronization of the high CAPE area and the variation of the CG lightning frequency between April and September in 2019 and 2020 (the same case can be found in the high KI area). Furthermore, the Pearson correlation coefficients of the CG lightning frequency with the high-value areas of the CAPE (above 200 J kg^{-1}) and KI (above 32 °C) both are 0.7, while the correlation coefficients of

the FY-4A-LMI lightning frequency with the high-value areas are lower than 0.1. These results indicate that the thermal instability conditions and the convective instability energy positively contribute the lightning activity for the CG observations, while the effect on the lightning activity for satellite-based observations is not obvious.

4 CONCLUSIONS AND DISCUSSION

Satellite-based detection of lightning efficiently supplements ground-based observations, expanding the detection field and providing additional resources for recognizing the distribution and variations of convective activities. Through the analyses of multi-year lightning observation data, it is evident that the lightning density distributions of the three data types are comparable, with higher values in central and southern Jiangxi, central Fujian, and central and western Guangdong but lower values in eastern Hunan. However, there are also some differences. The high-value areas of the FY-4A/LMI lightning density are located in inland mountainous areas. Notably, areas with lower latitudes exhibit higher lightning density, paralleling temperature distribution characteristics. The high-value areas of FY-4A/LMI lightning density are predominantly located in eastern Fujian and the southeastern coast of Zhejiang, and the high-value areas of the ISS-LIS lightning density are dispersed in inland mountainous areas and the coastline of eastern Fujian. The mountainous terrain is closely related to lightning-prone areas, and mountainsides or valleys are more conducive to lightning activity and its persistence. In the afternoon and evening, lightning density is moderately substantial in the inland areas of Jiangxi and near Dongting Lake in northern Hunan, while it is moderately weak in the mountainous areas around Jiangxi, most of Fujian and Zhejiang, and southern Hunan.

The seasonal variations in the lightning frequency and density for the FY-4A/LMI and CG observations show some similarities. In other words, the high-value areas for the two data types are mainly overlapped, and the variations are basically synchronous. In terms of the FY-4A/LMI observations, the evolutions of the mean wind field in the middle troposphere and vertical velocity in the lower troposphere are consistent with the lightning density distribution and lightning variation characteristics. In seasonal transitions, the variations of thermal and energy conditions have considerable effects on the lightning frequency variations. The lightning density variations for the FY-4A/LMI are consistent with the advance and retreat of the WPSH characterized by the prevailing wind in the middle layer. Moreover, the specific values of the KI and CAPE serve as reliable indicators, effectively reflecting the boundary of the high-value areas of lightning density and frequency. Thermal conditions represented by temperature and energy conditions depicted by CAPE can also indicate the seasonal variation characteristics of lightning. The CAPE and T_d are highly correlated with the CG lightning frequency, and their influence on the CG lightning is larger than that of air temperature. However, their correlations with the FY-4A/LMI and ISS-LIS lightning frequencies are weak.

The analyses of the long-term lightning data series from the FY-4A/LMI and ISS-LIS provide insights into convective activities in Jiangxi and its adjacent areas. Notably, there is a scarcity of relevant studies and achievements in both domestic and international contexts, rendering this work pioneering. The research results show that the ISS-LIS lightning data from the Global Hydrology Resource Center after quality control is evidently less than the FY-4A/LMI and CG lightning data, and the intermittent lightning frequency is two orders of magnitude lower than the CG lightning frequency. This phenomenon has been uncovered for the first time, and further investigations are warranted to ascertain its underlying causes. Additionally, the quality of the FY-4A/LMI lightning data decreases year by year, not only due to reduced precipitation in certain years but also due to the decay of the detection performance of the instrument, which needs further confirmation.

***Acknowledgements*:** We extend our sincere gratitude to the editor and anonymous reviewers, as their comments are all valuable and very helpful for improving the quality of this paper. We also thank Nanjing Hurricane Translation for reviewing the English language quality of this paper.

REFERENCES

[1] HOLLE R L, ZHANG D L. How lightning detection networks were developed in Arizona [J]. Flashes of Brilliance, 2023, 12: 153–174, https://doi.org/10.1007/978–3–031–19879–3_6

[2] CUMMINS K L, MURPHY M J. An overview of lightning locating systems: history, techniques, and data uses, with an in-depth look at the US NLDN [J]. IEEE Transactions on Electromagnetic Compatibility, 2009, 51(3): 499–518, https://doi.org/10.1109/TEMC.2009.2023450

[3] ZHANG Y J, ZHANG Y, ZOU M J, et al. Advances in lightning monitoring and location technology research in China [J]. Remote Sensing, 2022, 14(5): 1287–1293, https://doi.org/10.3390/rs14051293

[4] CHEN L W, ZHANG Y J, LYV W T, et al. Performance evaluation for a lightning location system based on observations of artificially triggered lightning and natural lightning flashes [J]. Journal of Atmospheric and Oceanic Technology, 2012, 29(12): 1835–1844, https://doi.org/10.1175/JTECH-D-12–00028.1

[5] LIU R X, LU Q F, CHEN M, et al. Quality assessment of FY-4A lightning data in inland China [J]. Journal of Tropical Meteorology, 2020, 26(3): 286–299, https://doi.org/10.46267/j.1006–8775.2020.026

[6] LYU W T, ZHEN D, ZHANG Y, et al. A review of atmospheric electricity research in China from 2019 to 2022 [J]. Advances in Atmospheric Sciences, 2023, 40(8): 1457–1484, https://doi.org/10.1007/s00376–023–2280-x

[7] BRUNING E C, TILLIER C E, EDGINGTON S F, et al. Meteorological imagery for the geostationary lightning

mapper [J]. Journal of Geophysical Research: Atmospheres, 2019, 124(24): 14285–14309, https://doi.org/10.1029/2019JD030874

[8] YANG J, ZHANG Z Q, WEI C Y, et al. Introducing the new generation of Chinese Geostationary Weather Satellites, Fengyun-4 [J]. Bulletin of the American Meteorological Society, 2017, 98(8): 1637–1659, https://doi.org/10.1175/BAMS-D-16–0065.1

[9] CAO D J, LU F, ZHANG X H, et al. Lightning activity observed by the FengYun-4A lightning mapping imager [J]. Remote Sensing, 2021, 13(15): 4922–4941, https://doi.org/10.3390/rs13153013

[10] HUI W, GUO Q. Preliminary characteristics of measurements from Fengyun-4A Lightning Mapping Imager [J]. Remote Sensing, 2021, 42(13): 4922–4941, https://doi.org/10.1080/01431161.2021.1906983

[11] LIU Y, WANG H B, ZHENG L, et al. A verification of the lightning detection data from FY-4A LMI as compared with ADTD-2 [J]. Atmospheric Research, 2021, 248(18): 105–163, https://doi.org/10.1016/j.atmosres.2020.105163

[12] ZHU J. Comparison of the satellite-based Lightning Imaging Sensor (LIS) against the ground-based national lightning monitoring network [J]. Progress in Geophysics, 2018, 33(2): 541–546, https://doi.org/10.6038/pg2018AA0631, in Chinese with English abstract

[13] VIRTS K, WALLACE J M, HUTCHINS M, et al. Diurnal lightning variability over the maritime continent: impact of low-level winds, cloudiness, and the MJO [J]. Journal of the Atmospheric Sciences, 2013, 70(10): 3128–3146, https://doi.org/10.1175/JAS-D-13–021.1

[14] KOCHTUBAJDA B, BURROWS W. Cloud-to-ground lightning in Canada: 20 years of CLDN Data [J]. Atmosphere-Ocean, 2020, 58(4): 1–17, https://doi.org/10.1080/07055900.2020.1845117

[15] ANTONESCU B, BURCEA S. A cloud-to-ground lightning climatology for Romania [J]. Monthly Weather Review, 2010, 138(2): 579–591, https://doi.org/10.1175/2009MWR2975.1

[16] KULESHOV Y. Thunderstorm and lightning climatology of Australia [J]. Modern Climatology, 2012, 11(3): 85–120, http://dx.doi.org/10.5772/35075

[17] YUAN T, QIE X S. Spatial and temporal distributions of lightning activities in China from satellite observation [J]. Plateau Meteorology, 2004, 23(4): 488–494, https://doi.org/10.3321/j.issn:1000–0534.2004.04.011, in Chinese with English abstract

[18] HOUZE R A, RASMUSSEN K L, ZULUAGA M D, et al. The variable nature of convection in the tropics and subtropics: A legacy of 16 years of the Tropical Rainfall Measuring Mission (TRMM) satellite [J]. Reviews of Geophysics, 2015, 53(3): 994–1021, https://doi.org/10.1002/2015RG000488

[19] BüRGESSER R E, MICORA M G, ÁVILA E E. Characterization of the lightning activity of "Relámpago del Catatumbo" [J]. Journal of Atmospheric and Solar-Terrestrial Physics, 2012, 77: 241–247, https://doi.org/10.1016/j.jastp.2012.01.013

[20] ORVILLE R E, HUFFINES G R, BURROWS W R, et al. The North American Lightning Detection Network (NALDN)-analysis of flash data: 2001–09 [J]. Monthly Weather Review, 2011, 139(5): 1305–1322, https://doi.org/10.1175/2010MWR3452.1

[21] LIOU Y A, KAR S K. Study of cloud-to-ground lightning and precipitation and their seasonal and geographical characteristics over Taiwan [J]. Atmospheric Research, 2010, 95(2–3): 115–122, https://doi.org/10.1016/j.atmosres.2009.08.016

[22] HUI W, HUANG F X, GUO Q. Combined application of lightning detection data from satellite and ground-based observations [J]. Optics and Precision Engineering, 2018, 26(1): 218–229, http://doi.org/10.3788/OPE.20182601.0218, in Chinese with English abstract

[23] WANG D F, QIE X S, YUAN S F, et al. Spatial and temporal distribution of lightning activity and contribution of thunderstorms with different lightning-producing capabilities in Beijing Metropolitan Region [J]. Chinese Journal of Atmospheric Sciences, 2020, 44(2): 225–238, https://doi.org/10.3878/j.issn.1006–9895.1904.19128, in Chinese with English abstract

[24] XIA R D, ZHANG D L, WANG B. A 6-yr cloud-to-ground lightning climatology and its relationship to rainfall over central and eastern China [J]. Journal of Applied Meteorology and Climatology, 2015, 54(12): 2442–2460, https://doi.org/10.1175/JAMC-D-15–0029.1, in Chinese with English abstract

[25] WANG Y G, LIU J, WANG J J, et al. Temporal and spatial distributions of lightning activity in Southwest China based on satellite observations [J]. Transactions of Atmospheric Sciences, 2010, 33(4): 489–495, https://10.3969/j.issn.1674–7097.2010.04.013, in Chinese with English abstract

[26] ZHENG Y G, CHEN J. A climatology of deep convection over South China and adjacent waters during summer [J]. Journal of Tropical Meteorology, 2013, 19(1): 1–15, https://api.semanticscholar.org/CorpusID:131472797, in Chinese with English abstract

[27] FENG G L, QIE X S, YUAN T, et al. Study on the characteristics of lightning activity and precipitation structure of hail storms [J]. Science in China Series D Earth Sciences, 2007, 37(1): 123–132, https://doi.org/10.1360/zd2007–37–1–123, in Chinese with English abstract

[28] XU W X. Thunderstorm climatologies and their relationships to total and extreme precipitation in China [J]. Journal of Geophysical Research: Atmospheres, 2020, 125(19): 1–19, https://doi.org/10.1029/2020JD033152

[29] ZHENG D, ZHANG Y J, MENG Q, et al. Climatology of lightning activity in South China and its relationships to precipitation and convective available potential energy [J]. Advances in Atmospheric Sciences, 2016, 33(3): 365–376, https://doi.org/10.1007/s00376–015–5124–5, in Chinese with English abstract

[30] YU H, ZHANG H B, LIU D X, et al. Relationship between lightning activities and radar echoes of squall line convective systems [J]. Chinese Journal of Atmospheric Sciences, 2022, 46(4): 835−844, http://doi.org/10.3878/j.issn.1006–9895.2101.20243, in Chinese with English abstract

[31] WANG Y, ZHANG Y J, MA M. Lightning activities in China offing sea area observed by satellite-based lightning imaging sensor [J]. Journal of Applied Meteorology and Climatology, 2010, 21(2): 157–163, https://doi.org/10.11898/1001–7313.20100204, in Chinese with English

abstract
[32] CAREY L D, RUTLEDGE S A, PETERSON W A. The relationship between severe storm reports and cloud-to-ground lightning polarity in the contiguous United States from 1989 to 1998 [J]. Monthly Weather Review, 2003, 131(7): 1211–1228, https://doi.org/10.1175/1520–0493(2003)131<1211:TRBSSR>2.0.CO;2
[33] XU G Q, HUANG S Y, ZHAO C Y. Influence of FY-4A lightning data on numerical forecast of convective weather [J]. Meteorological Monthly, 2020, 46(9): 1165–1177, https://doi.org/10.7519/j.issn.1000–0526.2020.09.004, in Chinese with English abstract
[34] REN S L, ZHAO W, CAO D J, et al. Application of FY-4A daytime convective storm and lightning products in analyzing severe thunderstorm weather in North China [J]. Journal of Marine Meteorology, 2020, 40(1): 33–46, https://doi.org/10.19513/j.cnki.issn2096–3599.2020.01.004, in Chinese with English abstract
[35] LI P F, ZHAI G F, PANG W J, et al. Preliminary research on a comparison and evaluation of FY-4A LMI and ADTD data through a moving amplification matching algorithm [J]. Remote Sensing, 2021, 13(1): 11, https://doi.org/10.3390/rs13010011
[36] WILLIAMS E R. The electrification of severe storms [M]// In Doswell C A (eds) Severe Convective Storms. Boston: American Meteorological Society, 2001, https://doi.org/10.1007/978–1–935704–06–5_13
[37] RUTLEDGE S A, WILLIAMS E R, KEENAN T D. The Down Under Doppler and Electricity Experiment (DUNDEE): overview and preliminary results [J]. Bulletin of the American Meteorological Society, 1992, 73(1): 3–16, https://doi.org/10.1175/1520–0477(1992)073<0003:TDUDAE>2.0.CO;2
[38] WILLIAMS E R, GEOTIS S G, RENNO N, et al. A radar and electrical study of tropical “hot towers” [J]. Journal of the Atmospheric Sciences, 1992, 49(15): 1386–1395, https://doi.org/10.1175/1520–0469(1992)049<1386:ARAESO>2.0.CO; 2

Citation: ZHI Shu-lin, ZHU Jie, LIU Yan, et al. Characteristics of Lightning Activity in Southeast China and its Relation to the Atmospheric Background [J]. Journal of Tropical Meteorology, 2024, 30(1): 76-88, https://doi.org/10.3724/j.1006-8775.2024.008